



# Performance bound for robust array calibration in radio interferometry

A Boudehane, Remy Boyer, V. Ollier, M Korso, A. Ferrari, P. Larzabal

## ► To cite this version:

A Boudehane, Remy Boyer, V. Ollier, M Korso, A. Ferrari, et al.. Performance bound for robust array calibration in radio interferometry. GRETSI 2019 - XXVIIème Colloque francophone de traitement du signal et des images, Aug 2019, Lille, France. hal-02141553

**HAL Id: hal-02141553**

**<https://hal.archives-ouvertes.fr/hal-02141553>**

Submitted on 28 May 2019

**HAL** is a multi-disciplinary open access archive for the deposit and dissemination of scientific research documents, whether they are published or not. The documents may come from teaching and research institutions in France or abroad, or from public or private research centers.

L'archive ouverte pluridisciplinaire **HAL**, est destinée au dépôt et à la diffusion de documents scientifiques de niveau recherche, publiés ou non, émanant des établissements d'enseignement et de recherche français ou étrangers, des laboratoires publics ou privés.

# PERFORMANCE BOUND FOR ROBUST ARRAY CALIBRATION IN RADIO INTERFEROMETRY

*A. Boudehane*<sup>1</sup>, *R. Boyer*<sup>2</sup>, *V. Ollier*<sup>3</sup>, *M. N. El Korso*<sup>4</sup>, *A. Ferrari*<sup>5</sup> and *P. Larzabal*<sup>6</sup>

<sup>1</sup> L2S, Université de Paris-Sud, Gif-sur-Yvette, France

<sup>2</sup> CRISAL, Université de Lille, France

<sup>3</sup> Safran Electronics & Defense, Eragny, France

<sup>4</sup> LEME, Université de Paris-Nanterre, Ville d'Avray, France

<sup>5</sup> Université Côte d'Azur, Observatoire de la Côte d'Azur, CNRS, Laboratoire Lagrange, France

<sup>6</sup> SATIE, ENS Paris-Saclay, Cachan, France

## ABSTRACT

Robust calibration of next-generation radio-interferometers, as the square kilometer array (SKA) for instance, is a crucial preprocessing step for sky imaging. Recently, several robust calibration estimators based on the use of well known strong sources in the field of view (FOV) have been proposed in the literature. For that, usually a compound-Gaussian (CG) noise is considered since it can take into account the presence of outliers, such that unknown weak sources in the FOV, and remains mathematically tractable. Specifically, the CG model is a zero-mean Gaussian process with a random variance, usually called texture. Performance bounds provide the lowest mean squared error (MSE) that an unbiased estimator can hope to reach. To the best of our knowledge, there is a lack of practical bounds dedicated to the robust calibration of future radio interferometers as far as they can be used as design tools for a given FOV. In this work, the hybrid Cramér-Rao bound (HCRB) is derived for a propagation model based on the Jones-matrix formalism corrupted by a CG noise for several texture distributions (K-distribution, Student's t, Cauchy, and Inverse-Gaussian compound Gaussian distribution (IG-CG)). In this standard physical model, the waveform propagation model is parametrized by a set of deterministic physical parameters of interest (complex gains, phases, DOA, etc.). In this work, we show that the HCRB w.r.t. the physical deterministic parameters is in fact given by the modified CRB (MCRB). The MCRB is easy to derive since only the first-order moment of the inverse of the texture variable is needed.

## 1 Introduction

Astronomical radio-waves cross different layers of the atmosphere and are subject to various distortions before reaching earth. Hence, sky imaging requires a robust estimation of the different parameters deforming the signal (delay, phase, complex gain-attenuation, etc.). The Jones-matrix formalism [12] is a widespread model of radio wave propagation, standing for all physical phenomena which affect the signal, from the source until the receiver.

Typically, the calibration process is performed based on the so-called calibration sources. It is worth mentioning that, in addition to the distortion introduced by the layers of the ionosphere, ambient Gaussian noise is present as well a number of unknown non-calibration sources interfering with known calibration sources, leading to unrealistic Gaussian noise assumption. Compound-Gaussian

(CG) noise model is, however, closer to reality taking in consideration these non-calibration sources.

Many calibration algorithms are found in literature, giving different scenario dependent efficiencies. S. Kazemi and S. Yatawatta [5] have first, introduced a student model to overcome the limitations inherent to a Gaussian framework. Recently, we have shown [8] that estimator based on compound Gaussian noise improves S. Kazemi and S. Yatawatta results thanks to the use of a more powerful and flexible distribution. Thereby, a new performance-evaluation reference is needed in order to convey this improvement.

The Cramér-Rao bound (CRB) is commonly used as a reference for evaluation of estimators. The classical CRB is a lower bound for unbiased estimators' variance. Other forms derived from the CRB (the estimated Cramér-Rao Bound ECRB, the modified Cramér-Rao Bound and the hybrid Cramér-Rao Bound) may be used as lower bounds on the MSE of estimators, such as the maximum a posteriori (MAP) used in [9] under a compound-Gaussian assumption of the noise. In this case, the noise is modeled as a zero mean complex Gaussian component with a positive random variable representing the texture. Taking into account this nuisance random parameter (texture) in the estimation process leads us to take it as well into consideration in the definition of the lower bound.

The notations used in this paper are the following:  $(\cdot)^T$ ,  $(\cdot)^H$ ,  $(\cdot)^*$ , stand, respectively, for the transpose, the transpose complex conjugate and the complex conjugate operators with  $j$  denoting the imaginary unit.  $\Re\{\cdot\}$  and  $\Im\{\cdot\}$  are, respectively, the real and the imaginary parts of a complex value.  $\mathbb{E}\{\cdot\}$  stands for the expectation while  $\text{VAR}(\cdot)$  and  $\text{COV}(\cdot)$  denote, respectively, the variance and the covariance. The Kronecker product is represented by  $\otimes$ , the trace operator by  $\text{tr}\{\cdot\}$ , the determinant by  $|\cdot|$  while  $\text{vec}(\cdot)$  denotes the vectorization (column stacking).

## 2 Model setup

The model setup given in [6] reduces to the use of a  $2 \times 2$  Jones matrix with the assumption of a plane-wave with two components of the electric field in  $xy$  plane, perpendicular to the direction of propagation  $z$ . The measured voltage at antenna  $p$  with a single source  $i$  is given by

$$\mathbf{v}_{i,p}(\boldsymbol{\theta}) = \mathbf{J}_{i,p}(\boldsymbol{\theta})\mathbf{s}_i. \quad (1)$$

in which the  $2 \times 1$  vector  $\mathbf{v}_{i,p} = [v_{i,p}^x, v_{i,p}^y]^T$  is the voltage measured in the two polarization directions  $x$  and  $y$ , the calibration source sig-

nal is given by  $\mathbf{s}_i = [s_i^x, s_i^y]$  and the  $2 \times 2$  Jones matrix  $\mathbf{J}_{i,p}(\boldsymbol{\theta})$  models the propagation from source  $i$  to antenna  $p$ . Each Jones matrix is parametrized by the unknown vector  $\boldsymbol{\theta}$  representing all the distortions along the propagation path [12]. This standard waveform propagation model, defined in [10], is given for the  $p$ -th antenna and the  $i$ -th source by:

$$\mathbf{J}_{i,p}(\boldsymbol{\theta}) = \mathbf{G}_p(\mathbf{g}_p)\mathbf{H}_{i,p}\mathbf{Z}_{i,p}(\phi_{i,p})\mathbf{F}_i(\vartheta_{i,p}) \quad (2)$$

where

- $\mathbf{G}_p(\mathbf{g}_p) = \text{diag}\{\mathbf{g}_p\}$  is a  $2 \times 2$  diagonal matrix that represents the antenna complex gain, with  $\mathbf{g}_p = [[\mathbf{g}_p]_1, [\mathbf{g}_p]_2]^T$ .
- $\mathbf{Z}_{i,p}(\phi_{i,p}) = \exp\{j\phi_{i,p}\}\mathbf{I}_2$  represents the ionospheric phase with  $\mathbf{I}_2$  the  $2 \times 2$  identity matrix.
- The Faraday rotation effect is represented by

$$\mathbf{F}_i(\vartheta_{i,p}) = \begin{bmatrix} \cos \vartheta_{i,p} & -\sin \vartheta_{i,p} \\ \sin \vartheta_{i,p} & \cos \vartheta_{i,p} \end{bmatrix}.$$

- Finally, the known  $2 \times 2$  matrix  $\mathbf{H}_{i,p}$  is obtained thanks to electromagnetic simulations and represents antenna response [9].

The ordered global output vector reads

$$\mathbf{x} = [\mathbf{x}_{12}^T \quad \mathbf{x}_{13}^T \quad \mathbf{x}_{23}^T \quad \cdots \quad \mathbf{x}_{(M-1)M}^T]^T. \quad (3)$$

where  $M$  denotes the total number of antennas and  $L = \frac{M(M-1)}{2}$  is the number of possible antenna pairs. Each  $4 \times 1$  subvector of  $\mathbf{x}$ , *i.e.*, for a given antenna pair  $(p,q)$ , is given by

$$\mathbf{x}_{pq} = \mathbf{v}_{pq} + \mathbf{n}_{pq} \quad (4)$$

where the signal and noise contributions denoted by  $\mathbf{v}_{pq}$  and  $\mathbf{n}_{pq}$ , respectively, are described in the two next paragraphs.

## 2.1 Cross-correlations measurement

The deterministic physical parameters of interest for  $D$  sources are collected in a  $K \times 1$  vector with  $K = 2MD + 4M$  given by

$$\boldsymbol{\theta} = [\boldsymbol{\vartheta}^T, \boldsymbol{\phi}^T, \mathbf{g}^T]^T \quad (5)$$

where the  $(MD) \times 1$  vector  $\boldsymbol{\vartheta} = [\vartheta_1^T \dots \vartheta_M^T]^T$  with  $\vartheta_p = [\vartheta_{1,p} \dots \vartheta_{D,p}]^T$  ( $D \times 1$  vector) collect the Faraday angles per source (index  $i$ ) per antenna (index  $p$ ) while  $\boldsymbol{\phi} = [\phi_1^T \dots \phi_M^T]^T$  with  $\phi_p = [\phi_{1,p} \dots \phi_{D,p}]^T$  is the ionospheric phase delay for the  $i$ -th source and the  $p$ -th antenna. One assumes a  $D \times M$  source and receiver dependent ionospheric parameter vector. Finally,  $\mathbf{g}_p = [\Re\{\mathbf{g}_p\}_1, \Im\{\mathbf{g}_p\}_1, \Re\{\mathbf{g}_p\}_2, \Im\{\mathbf{g}_p\}_2]^T$  represents direction independent antenna gain after vectorization of both real and imaginary parts.

Interferometers measure the cross-correlations of antenna pairs [6]. The correlation measurement for antennas  $p$  and  $q$  is written as

$$\begin{aligned} \mathbf{V}_{pq}(\boldsymbol{\theta}) &= \mathbb{E} \left\{ \left( \sum_{i=1}^D \mathbf{v}_{i,p}(\boldsymbol{\theta}) \right) \left( \sum_{i=1}^D \mathbf{v}_{i,q}^H(\boldsymbol{\theta}) \right) \right\} \\ &= \sum_{i=1}^D \mathbf{J}_{i,p}(\boldsymbol{\theta}) \mathbf{C}_i \mathbf{J}_{i,q}^H(\boldsymbol{\theta}) \end{aligned} \quad (6)$$

where  $\mathbf{C}_i = \mathbb{E}\{\mathbf{s}_i \mathbf{s}_i^H\}$  is the  $2 \times 2$  source coherency matrix [6]. Using [7, eq. 82], an equivalent vectorized expression of eq. (6) is given by

$$\mathbf{v}_{pq}(\boldsymbol{\theta}) = \text{vec}(\mathbf{V}_{pq}(\boldsymbol{\theta})) = \sum_{i=1}^D (\mathbf{J}_{i,q}^*(\boldsymbol{\theta}) \otimes \mathbf{J}_{i,p}(\boldsymbol{\theta})) \mathbf{c}_i \quad (7)$$

where  $\mathbf{c}_i = \text{vec}(\mathbf{C}_i)$  is the  $4 \times 1$  vector obtained by vectorizing the  $i^{\text{th}}$  source coherency matrix (column stacking).

## 2.2 Non-Gaussian noise modeling

The noise is assumed to follow a compound-Gaussian distribution with two components: a zero mean complex Gaussian component and a texture representing the effect of non-calibration sources interference [13]. Hence,  $\mathbf{n}_{pq} = \sqrt{\tau_{pq}} \mathbf{u}_{pq}$  where  $\tau_{pq}$  is a positive real random variable representing the texture and  $\mathbf{u}_{pq}$  is a  $4 \times 1$  vector following a zero-mean circular Gaussian distribution, *i.e.*,  $\mathbf{u}_{pq} \sim \mathcal{CN}(\mathbf{0}, \boldsymbol{\Omega})$  where  $\boldsymbol{\Omega}$  is the noise covariance matrix. The noise vector (sorted accordingly with  $\mathbf{x}$  in eq. (3)) is

$$\mathbf{n} | \boldsymbol{\tau} \sim \mathcal{CN}(\mathbf{0}, \boldsymbol{\Gamma}) \quad (8)$$

where

$$\boldsymbol{\Gamma} = \mathbf{T} \otimes \boldsymbol{\Omega} \quad (9)$$

in which  $\mathbf{T} = \text{diag}(\boldsymbol{\tau})$  is the  $L \times L$  texture matrix with  $\boldsymbol{\tau} = [\tau_{11} \dots \tau_{(M-1)M}]^T$ . Statistical priors on  $\boldsymbol{\tau}$  as K-distribution, Student's t, Cauchy, Laplace and Inverse-Gaussian Compound Gaussian distribution (IG-CG) are considered in the sequel [9].

## 3 Hybrid set of parameters

### 3.1 Deterministic and random parameters

- The deterministic physical parameters of interest are collected in  $\boldsymbol{\theta}$  defined in section 2.1.1.
- The unknown nuisance parameters are represented by the random texture vector  $\boldsymbol{\tau}$  defined in section 2.1.2.

Let  $\hat{\boldsymbol{\theta}}'$  be an estimate vector of the hybrid parameter of interest vector, *i.e.*,  $\boldsymbol{\theta}' = [\boldsymbol{\tau}^T, \boldsymbol{\theta}^T]^T$ . A key fidelity measure for any estimator is the MSE defined by

$$\text{MSE}(\hat{\boldsymbol{\theta}}') = \mathbb{E}_{\boldsymbol{\tau}} \mathbb{E}_{\mathbf{x} | \boldsymbol{\tau}} \|\hat{\boldsymbol{\theta}}'(\mathbf{x}) - \boldsymbol{\theta}'\|^2. \quad (10)$$

### 3.2 Hybrid lower bound

In this part, we focus on the HCRB which is the most realistic, since it is derived considering the deterministic and the random parameters. The HCRB matrix, denoted by  $\mathbf{C}_{\mathcal{H}}(\boldsymbol{\theta}')$ , is a lower bound on the MSE for any estimator  $\hat{\boldsymbol{\theta}}'$  according to the following inequality:

$$\text{tr}\{\mathbf{C}_{\mathcal{H}}(\boldsymbol{\theta}')\} \leq \text{MSE}(\hat{\boldsymbol{\theta}}'). \quad (11)$$

Specifically,  $\mathbf{C}_{\mathcal{H}}(\boldsymbol{\theta}')$  is defined as the inverse matrix of the Hybrid Information Matrix (HIM) [2] given by

$$\mathbf{F}_{\mathcal{H}}(\boldsymbol{\theta}') = \mathbf{F}_{\text{det}}(\boldsymbol{\theta}') + \mathbf{F}_{\text{prior}}(\boldsymbol{\tau}) \quad (12)$$

where

$$\mathbf{F}_{\text{det}}(\boldsymbol{\theta}') = \mathbb{E}_{\boldsymbol{\tau}} \left\{ \mathbb{E}_{\mathbf{x} | \boldsymbol{\theta}'} \left\{ -\Delta_{\boldsymbol{\theta}'} \log P(\mathbf{x} | \boldsymbol{\tau}; \boldsymbol{\theta}') \right\} \right\} \quad (13)$$

in which  $[\Delta_{\alpha}^{\beta} g(\cdot)]_{i,j} = \frac{\partial^2 g(\cdot)}{\partial[\alpha]_i \partial[\beta]_j}$ ,

$$\mathbf{F}_{\text{prior}}(\boldsymbol{\tau}) = \begin{bmatrix} \mathbf{F}'_{\text{prior}}(\boldsymbol{\tau}) & \mathbf{0} \\ \mathbf{0} & \mathbf{0} \end{bmatrix} \quad (14)$$

and

$$\mathbf{F}'_{\text{prior}}(\boldsymbol{\tau}) = \mathbb{E}_{\boldsymbol{\tau}} \{-\Delta_{\boldsymbol{\tau}}^{\boldsymbol{\tau}} \log P(\boldsymbol{\tau})\}. \quad (15)$$

### 3.2.1 Link to the Modified CRB

A comparison and links between different forms of the CRB, among which the HCRB and the MCRB, have been defined in [14]. In our context, we provide in the following lemma a key technical result on the HCRB.

**Lemma 1** *The HCRB matrix is block-diagonal, i.e., parameters  $\boldsymbol{\theta}$  and  $\boldsymbol{\tau}$  are decoupled.*

**Proof 1** *As  $\mathbf{x}|\boldsymbol{\tau} \sim \mathcal{CN}(\boldsymbol{\mu}, \boldsymbol{\Gamma})$ , the conditional log-likelihood function reads [9]:*

$$\log P(\mathbf{x}|\boldsymbol{\tau}; \boldsymbol{\theta}) = -\log(|\pi\boldsymbol{\Gamma}|) - \mathbf{w}^H \boldsymbol{\Gamma}^{-1} \mathbf{w} \quad (16)$$

where  $\mathbf{w} = \mathbf{x} - \boldsymbol{\mu}$ . The coupling terms between  $\boldsymbol{\theta}$  and  $\boldsymbol{\tau}$ , are given by

$$\Delta_{\boldsymbol{\theta}}^{\boldsymbol{\tau}} \log P(\mathbf{x}|\boldsymbol{\tau}; \boldsymbol{\theta}) = \frac{\partial \boldsymbol{\mu}^H}{\partial \boldsymbol{\theta}} \frac{\partial \boldsymbol{\Gamma}^{-1}}{\partial \boldsymbol{\tau}} \mathbf{w} + \mathbf{w}^H \frac{\partial \boldsymbol{\Gamma}^{-1}}{\partial \boldsymbol{\tau}} \frac{\partial \boldsymbol{\mu}}{\partial \boldsymbol{\theta}}. \quad (17)$$

Since  $\mathbb{E}_{\mathbf{x}|\boldsymbol{\tau}}(\mathbf{w}) = \mathbf{0}$ , we have

$$\mathbb{E}_{\mathbf{x}|\boldsymbol{\tau}} \{-\Delta_{\boldsymbol{\theta}}^{\boldsymbol{\tau}} \log P(\mathbf{x}|\boldsymbol{\tau}; \boldsymbol{\theta})\} = \mathbf{0}. \quad (18)$$

**Theorem 1** *The lower bound on the parameters of interest  $\boldsymbol{\theta}$  can be easily derived according to the well-known Modified CRB (MCRB) [3].*

**Proof 2** *As a consequence of lemma 1, eq. (13) can be written as*

$$\mathbf{F}_{\text{det}}(\boldsymbol{\theta}) = \mathbb{E}_{\boldsymbol{\tau}} \mathbb{E}_{\mathbf{x}|\boldsymbol{\tau}} \left\{ -\Delta_{\boldsymbol{\theta}}^{\boldsymbol{\theta}} \log P(\mathbf{x}|\boldsymbol{\tau}, \boldsymbol{\theta}) \right\} \quad (19)$$

and its inverse matrix denoted by  $\mathbf{C}_{\mathcal{M}}(\boldsymbol{\theta})$  is the well-known MCRB matrix [3]. Equivalently, the HCRB matrix is given by:

$$\mathbf{C}_{\mathcal{H}} = \begin{bmatrix} \mathbf{F}'_{\text{prior}}^{-1} & \mathbf{0} \\ \mathbf{0} & \mathbf{C}_{\mathcal{M}} \end{bmatrix}. \quad (20)$$

This result is important since closed-form expressions with respect to the texture parameter would be easily obtained with the MCRB. On the other hand, it is difficult to obtain closed-form expressions with the Expected CRB (ECRB) [4]. This bound is defined as:

$$\mathbf{C}_{\mathcal{E}}(\boldsymbol{\theta}) = \mathbb{E}_{\boldsymbol{\tau}} \left( \mathbb{E}_{\mathbf{x}|\boldsymbol{\tau}} \left\{ -\Delta_{\boldsymbol{\theta}}^{\boldsymbol{\theta}} \log P(\mathbf{x}|\boldsymbol{\tau}, \boldsymbol{\theta}) \right\} \right)^{-1}. \quad (21)$$

Indeed, in the expression above, the derivation in a closed-form of the expectation over  $\boldsymbol{\tau}$  is a delicate problem since this step is done after a matrix inversion. More precisely, in the ECRB approach, the generic form of the expressions involving the texture parameter is  $\mathbb{E}_{\boldsymbol{\tau}}(f(\boldsymbol{\tau}))$  where function  $f(\cdot)$  due to the matrix inversion is generally mathematically intractable. On the contrary, we show in the following that the function  $f(\cdot)$  is simple for the MCRB.

## 3.3 Closed-form expressions of the MCRB for different texture priors

### 3.3.1 General expression

As  $\mathbf{x}|\boldsymbol{\tau} \sim \mathcal{CN}(\boldsymbol{\mu}, \boldsymbol{\Gamma})$  or equivalently, the observation conditionally to the texture vector follows a complex Gaussian distribution, the Modified FIM is given by the expectation over the texture of the Slepian-Bangs formula [11], i.e.,

$$\mathbf{F}_{\text{det}}(\boldsymbol{\theta}) = 2\Re\{\mathbf{U}^H \mathbb{E}_{\boldsymbol{\tau}}(\boldsymbol{\Gamma}^{-1}) \mathbf{U}\} \quad (22)$$

where  $\mathbf{U} = \frac{\partial \boldsymbol{\mu}}{\partial \boldsymbol{\theta}^T}$  and

$$\mathbb{E}_{\boldsymbol{\tau}}(\boldsymbol{\Gamma}^{-1}) = \mathbb{E}_{\boldsymbol{\tau}}(\mathbf{T}^{-1}) \otimes \boldsymbol{\Omega}^{-1}. \quad (23)$$

### 3.3.2 Texture priors

According to [9], it is realistic to assume that texture  $\tau_{pq}$  follows a distribution parametrized by a set of hyper-parameters independent from the antenna pairs. Under this mild assumption, we are interested by the first moment of the random variable  $T_{pq} = \frac{1}{\tau_{pq}}$ , denoted by  $m_T^{(1)}$ . Thus the MCRB matrix is given by

$$\mathbf{C}_{\mathcal{M}}(\boldsymbol{\theta}) = \frac{1}{2m_T^{(1)}} \left[ \Re\{\mathbf{U}^H (\mathbf{I} \otimes \boldsymbol{\Omega}^{-1}) \mathbf{U}\} \right]^{-1}. \quad (24)$$

As we see, the MCRB matrix is the product of two terms. The first one  $\frac{1}{2m_T^{(1)}}$  is characterized by the choice of the texture prior and the second one,  $[\Re\{\mathbf{U}^H (\mathbf{I} \otimes \boldsymbol{\Omega}^{-1}) \mathbf{U}\}]^{-1}$ , is texture-independent. Let us remark that regarding the ECRB, it is not possible to obtain a ‘‘physically’’ interpretable characterization.

**K-distribution** If the noise follows a K-distribution then  $\tau_{pq} \sim \text{Gamma}(a, b)$ . Thus,  $T_{pq} \sim \text{InvGamma}(a, \frac{1}{b})$  and thus

$$m_T^{(1)} = \frac{1}{b(a-1)}. \quad (25)$$

**Student’s t distribution** If the noise follows a Student’s t distribution, the texture  $\tau_{pq} \sim \text{InvGamma}(a, b)$ . This means that  $T_{pq} \sim \text{Gamma}(a, \frac{1}{b})$  and

$$m_T^{(1)} = \frac{a}{b}. \quad (26)$$

**Cauchy distribution** If the noise follows a Cauchy distribution, in this case,  $\tau_{pq} \sim \text{InvGamma}(1, b)$ . The distribution of  $T_{pq}$  follows an Exponential distribution of rate  $b$  (special case of Gamma) and

$$m_T^{(1)} = \frac{1}{b}. \quad (27)$$

**Inverse-Gaussian Compound-Gaussian** In this case, the texture  $\tau_{pq}$  follows an Inverse Gaussian distribution (Wald distribution) with a unit mean, i.e.  $\tau_{pq} \sim \mathcal{IG}(1, \lambda)$ . So,  $T_{pq}$  follows a reciprocal inverse Gaussian distribution, i.e.  $T_{pq} \sim \mathcal{RIG}(1, \lambda)$  [1] and

$$m_T^{(1)} = 1 + \frac{1}{\lambda}. \quad (28)$$

### 3.3.3 Simulation

In order to visualize the MCRB for the different texture priors, we consider  $D = 3$  calibration sources with  $M = 8$  receivers. For K-distribution, Student's t and Cauchy cases, the shape and the scale parameters of the texture distribution are  $a = 3$  and  $b = 2$ , respectively, while we consider  $\lambda = 0.5$  for the inverse-Gaussian compound-Gaussian case.

The source signals as well as the parameters of the Jones-matrices are randomly generated, with entries following the uniform distribution, with respect to the physical nature of each parameter, *i.e.*, for the Faraday rotation angles and the ionospheric phase, a randomly generated number following the uniform distribution is multiplied by  $\pi$  in order to get a radian angle in the gap  $[0, \pi]$ . Thus, the complex quantities, such as the complex gain, is generated so that both the real and the imaginary parts follow the uniform distribution.

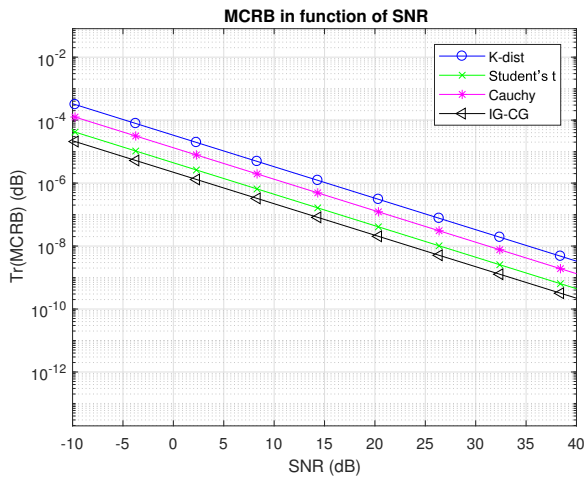


**Fig. 1.** Evolution of the trace of the MCRB in (dB) in function of the signal to noise ratio (SNR) in (dB) for the different kinds of prior in the Compound-Gaussian distribution.

In figure 1, we plot the trace of the MCRB (dB) in function of the signal to noise ratio (SNR) in (dB) for the different kinds of compound-Gaussian priors on the texture, *i.e.* for different kinds of compound-Gaussian distributions. The choice of the prior can thus be easily discussed, depending only the first moment  $m_T^{(1)}$  of the random variable  $T_{pq}$ , that defines the tightness of the bound for each prior.

## 4 Conclusion

In this paper, we defined the tractable lower bound on the MSE for a model with non-Gaussian noise used in robust array calibration for radio-interferometers. A compound-Gaussian (GC) assumption was considered on the noise, consisting of a zero mean complex Gaussian component and a random variable representing the texture, with different priors on the texture. In order to define the lower bound, we derived a hybrid form of the Cramér-Rao bound (HCRB) regarding the deterministic physical parameters of interest as well as the random parameters of nuisance (texture). The derivation of the HCRB gave us, as a result, a decoupling between the deterministic and the random parameters, leading to an equality between the HCRB and

the modified Cramér-Rao bound (MCRB) for the deterministic parameters of interest. This result allowed us to settle for the calculation of the MCRB, for the different priors on the texture, that we simulated as well. Generally speaking, this paper opens the way to the introduction of tractable minimal bounds for design tools in radio astronomy.

## References

- [1] O. E. Barndorff-Nielsen and A. E. Koudou. *Trees with Random Conductivities and the (Reciprocal) Inverse Gaussian Distribution*. Northern Ireland: Applied Probability Trust, 1998.
- [2] K. L. Bell and H. L. Van Trees. "Posterior Cramer-Rao Bound For Tracking Target Bearing". In: *Wiley-IEEE Press* (2007).
- [3] F. Gini, R. Reggiannini, and U. Mengali. "The Modified Cramer-Rao Bound in Vector Parameter Estimation". In: *IEEE Transactions on Communications* (1998).
- [4] Q. He and R. S. Blum. "The Significant Gains From Optimally Processed Multiple Signals of Opportunity and Multiple Receive Stations in Passive Radar". In: *IEEE Signal Processing Letters* (2014).
- [5] S. Kazemi and S. Yatawatta. "Robust radio interferometric calibration using the t-distribution". In: *Monthly Notices of the Royal Astronomical Society* (2013).
- [6] L. M. Ker. "Radio AGN Evolution with Low Frequency Radio Surveys, Ph.D. thesis". In: *University of Edinburgh* (2012).
- [7] H. D. Macedo and J. N. Oliveira. "Typing linear algebra: A biproduct-oriented approach". In: *ELSEVIER* (2012).
- [8] V. Ollier, M. N. El Korso, R. Boyer, P. Larzabal, and M. Pesavento. "Robust Calibration of Radio Interferometers in Non-Gaussian Environment". In: *IEEE Transactions on Signal Processing* (2017).
- [9] V. Ollier, M. N. El Korso, A. Ferrari, R. Boyer, and P. Larzabal. "Bayesian Calibration Using Different Prior Distributions: An Iterative Maximum a Posteriori Approach for Radio Interferometers". In: *EUSIPCO* (2018).
- [10] O. M. Smirnov. "Revisiting the radio interferometer measurement equation I. A full-sky Jones formalism". In: *Astronomy Astrophysics, vol. 527, no. A106* (2011).
- [11] P. Stoica and R. Moses. *SPECTRAL ANALYSIS OF SIGNALS*. Upper Saddle River, New Jersey 07458: PRENTICE HALL, 2004.
- [12] A. R. Thompson, J. M. Moran, and G. W. Swenson Jr. *Interferometry and Synthesis in Radio Astronomy. Second edition*. New York: John Wiley Sons, New York, 2012.
- [13] J. Wang, A. Dogandzic, and A. Nehorai. "Maximum Likelihood Estimation of Compound-Gaussian Clutter and Target Parameters". In: *IEEE Transactions on Signal Processing* (2006).
- [14] X. Zhang, M. N. El Korso, and M. Pesavento. "MIMO radar target localization and performance evaluation under SIRP clutter". In: *Signal Processing Journal, Elsevier, Volume 130* (2017).